Synthesis, Characterization, and Molecular Dynamics Simulation Of $Na_2O-CaO-SiO_2-ZnO$ Glasses

G. Lusvardi, G. Malavasi, L. Menabue,*,† and M. C. Menziani*,‡

Department of Chemistry, University of Modena e Reggio Emilia, Via Campi 183, 41100 Modena, Italy

Received: February 1, 2002; In Final Form: July 17, 2002

The glass of composition $Na_2O{\cdot}CaO{\cdot}2SiO_2$ was modified upon addition of ZnO to obtain the series of glasses $Na_2O{\cdot}CaO{\cdot}2SiO_2{\cdot}x$ZnO ($x = 0.17, 0.34, 0.68$), where $x = 0.68$ is the experimentally determined maximum zinc content that does not produce phase separation. The glasses were investigated by means of density and thermal measurements (glass-transition and crystallization temperatures); moreover, the phases separated upon crystallization were identified. The results of molecular dynamics (MD) simulations combined with the analysis of the crystal structure of the main phases separated ($Na_2Ca(SiO_3)_2$ and Na_2ZnSiO_4) provided insights into the structural role of zinc and its effect on the short- and medium-range order of the glass structures.

Introduction

Zinc-containing glasses have received much attention from researchers because of their improved final glass properties, such as chemical durability and mechanical properties in the case of silicate and borosilicate glasses[1] and low softening point and low melting point in the case of phosphate glasses.[2] This behavior has been justified on the basis of the structural role of the zinc ion in the glass network. The Zn^{2+} ion is known to present two common coordination geometries in oxygenated species: tetrahedral and octahedral. Preferences in the geometry to adopt are dictated by environmental factors. In fact, according to the crystal field theory of coordination compounds, the peculiar $3d^{10}$ electronic configuration of Zn^{2+} does not favor the octahedral coordination with respect to the tetrahedral one, at variance with that normally found for other first-transition divalent ions. Therefore, zinc ions are found in four-coordinated tetrahedral geometry, that is, Zn_2SiO_4 (at atmospheric pressure[3]) and ZnO,[4] and in hexa-coordinated octahedral geometry, i.e., Zn_2SiO_4, (at high pressure[5]) or in zinc−carboxylate complexes.[6]

The Zachariasen and Warren theory of glass[7] is in agreement with the crystal field theory and classifies Zn^{2+} as an intermediate species because it can adopt either the tetrahedral or the octahedral geometry, the first being typical of glass network formers and the second one of modifiers. This can be quantified on the basis of the field strength value, Z/a^2, defined by the Dietzel theory of glass[7] (Z = ion charge and a = M−O bond distance in the M_nO_m oxide). The network modifier ions fall in the 0.1−0.4 Z/a^2 range and the former ions in the 1.3−2.0 one. The field strength of $Zn^{2+} = 0.53$ (calculated on the basis of Zn−O = 1.95 Å[4]) can reasonably classify it as an intermediate ion. The main factor in determining the prevailing role of the zinc ion in the glass structure is considered the alkali oxide content.[8] At high alkali oxide content, zinc ions were found essentially tetrahedrally coordinated, and the alkali oxide supplies the oxygen atoms that are necessary to attain corner-sharing ZnO_4 tetrahedra;[9] a decrease in the concentration of tetrahedral zinc and an increase in the concentration of octahedral zinc were found with increasing of the zinc content. Other experimental results have given evidence of zinc tetrahedral geometry in binary phosphate glasses[10] and in borosilicate glasses,[1] while both octahedral and tetrahedral coordinations were adopted in silicate glasses of composition $ZnO{\cdot}3SiO_2$.[3]

The coordination behavior of zinc ions in binary silicate and ternary alkalisilicate glasses has been investigated by molecular dynamics (MD) simulations.[3,11] The local environmental structures obtained by using the modified Born−Mayer−Huggins (BMH) potentials[12] were found to be in good agreement with extended x-ray absorption fine structure (EXAFS) data on the same glasses and crystalline zinc silicates, indicating MD simulations to be a powerful tool for deciphering the local features around individual ions and helping the understanding of glass properties. However, until now no quaternary zinc-containing glasses have been investigated by MD simulations. Here, we report the results of an integrated experimental and theoretical study of the glasses of composition $Na_2O{\cdot}CaO{\cdot}2SiO_2{\cdot}x$ZnO ($x = 0.00, 0.17, 0.34, 0.68$), where $x = 0.68$ is the experimentally determined maximum zinc content that allows the formation of a homogeneous glass. The short- and medium-range order description of the glass structures, obtained by calculations based on the Buckingham potential, has been correlated with the experimental data measured for density, thermal analysis, and structural information of the crystal species obtained upon glass crystallization.

Experimental Section

Glass Preparation. Three different zinc-containing glasses and the reference glass corresponding to N25C25S50[13] (hereafter named S50) were prepared. About 100 g of batch was obtained by mixing reagent grade Na_2CO_3, $CaCO_3$, SiO_2, and $ZnCO_3$ raw materials in a sealed polyethylene bottle for 1 h. Premixed batches were put into a 50 mL platinum crucible and melted in electric oven for 2 h at 1550 °C. The melts were poured into stainless steel plates and after were ball milled in agate mill jars and sieved through 70 mesh and 32 mesh screen to produce a particle size range of 250 and 500 μm. The prepared glasses with their experimental compositions are reported in Table 1.

Glass Characterization. Scanning electron microscopy (SEM) observation and energy-dispersive spectrometry (EDS)

* To whom correspondence should be addressed.
† E-mail: menabue@unimo.it.
‡ E-mail: menziani@unimo.it. Tel: +39 059 2055091. Fax: +39 059 373543.

10.1021/jp020321s CCC: $22.00
Published on Web 08/29/2002

TABLE 1: Batch Compositions (mol %) from the General Glass Formula $Na_2O{\cdot}CaO{\cdot}2SiO_2{\cdot}xZnO$

oxide	$x = 0$ (S50)	$x = 0.17$	$x = 0.34$	$x = 0.68$
SiO_2	48.7	47.0	45.4	42.6
Na_2O	25.3	24.2	23.4	21.4
CaO	26.0	24.6	23.2	21.5
ZnO		4.2	8.0	14.5

TABLE 2: Density, Total Atoms Number, and Cell Size of the Simulation Box for the Investigated Glasses

composition	density (g/cm^3) (± 0.002)	atom number	cell size (Å)
$x = 0$ (S50)	2.718	1188	25.04
$x = 0.17$	2.810	1245	25.40
$x = 0.34$	2.894	1286	25.64
$x = 0.68$	3.028	1332	25.87

analysis by a Philips XL 40 scanning electron microscope were done on the as-quenched glasses and after the thermal treatment. Glass-transition temperature, T_g, values were determined by differential scanning calorimetry (DSC) analysis; crystallization temperature (T_c) and melting point were determined by means of differential thermal analysis (DTA).

DTA measurements were performed in air with a NETZSCH simultaneous thermal analyzer STA 409 instrument by using ~100 mg of sample previously finely milled to 108−125 μm particle size range. The scan rate was fixed to 10 °C/min, and the temperature range was 25−1200 °C.

DSC measurements were performed in air with a Perkin-Elmer DSC4 instrument by using ~40 mg of sample previously finely milled to 108−125 μm particle size range. The scan rate was fixed to 10 °C/min, and the temperature range was 25−600 °C. Density was determined with a Picnometer AccUPyc 1330 (Micromeritics) instrument at room temperature with accuracy of 0.002 g/cm^3. Each value is an average of three independent measurements. X-ray diffraction (XRD) analysis was performed on the as-quenched glasses and after the thermal treatment. XRD analyses were carried out on finely powdered samples with a Philips PW3710-based automated diffractometer using Ni-filtered Cu Kα radiation ($\lambda = 1.540\,60$ Å) in the $10° \le 2\theta \le 70°$ range with a step size of 0.02° and a time step of 6 s.

The calculation of structural parameters on Na_2ZnSiO_4 were performed by means of the program package Parst.[14]

Computational Procedure. MD simulations were performed with the DL_POLY program[15] at CICAIA (Centro Interdipartimentale di Calcolo Automatico e Informatica Applicata) of Modena and Reggio E. University, using Cerius2[16] as a graphical interface.

The input structures for the glass compositions experimentally characterized in this work were obtained by adding randomly the appropriate number and type of atoms into the simulation box of around 25 Å edge length (Table 2). The starting volume of the systems was increased up to 30% to account for the estimate thermal expansion coefficient and then scaled to reproduce the experimental density at the final simulation temperature. The long-range electrostatic potential was evaluated by the Ewald summation method with the cutoff distance set at 12 Å and precision set to 10^{-6}. The short-range cutoff distance was set at 7.6 Å. Periodic boundary conditions were applied to the simulations box. The short-range interactions between Si−O and Zn−O were modeled by using a four-range Buckingham potential model including O−Si−O three-body screened Vessal potential.[17] No constraints were explicitly considered for the O−Zn−O linkages to avoid assumptions on the coordination number of Zn. A simple Buckingham potential codifies the Na−O and Ca−O short-range interactions. The potential parameters used are listed in Table 3 and were taken from A. N. Cormack and Y. Cao[18] and G. V. Lewis and C. R. A. Catlow.[19]

TABLE 3: Buckingham Pair Potential Parameters Used in the MD Calculations

	$U(r) = A\,[\exp(-r/\rho)] - (C/r^6)$			
	A (eV)	ρ (Å)	C (eV Å^{-6})	ref
O−O	3 116 130.6	0.1515	61.3916	18
Si−O	1036.89	0.3259	0.0	18
Na−O	1226.8	0.3065	0.0	18
Ca−O	1228.9	0.3118	0.0	18
Zn−O	700.3	0.3372	0.0	19

The initial structures were melted at 12 000 K to remove possible memory effects and then cooled sequentially to 10 000, 8000, 6000, 3000, 1500, and finally to 300 K. At each temperature a 20 000 time steps relaxation was allowed at a time step of 2 fs. During the first 6000 of these 20 000 time steps, the velocity was scaled every time step. During the second 6000 time steps, velocity scaling every 40 time steps was performed, and finally, during the last 8000 time steps, no velocity scaling was applied. The canonical ensemble *NVT* (Evans thermostat) for constant number of particles, volume, and temperature was used. This annealing protocol was optimized in a previous work[20] on zirconium-containing glasses and represents a compromise between accuracy and computational requirements.

Data collection was performed every 10 time steps during the last 1500 time steps of the MD run. An additional 10.000 time step simulation was performed for the glass of composition $x = 0.17$ to test the dependence of the results upon the data collection time. No significant differences (less than 1%) were obtained for the CN and bond length distributions of the different species. Therefore, the annealing procedure used produces a stable trajectory.

Results and Discussion

The ZnO maximum content added to S50 that enables a homogeneous glass to be obtained was 14.5 mol % (corresponding to 18.5 wt %). In fact, the attempt of obtaining a glass with ZnO content of 15.5 mol % (corresponding to 20 wt %) was unsuccessful. The composition of the prepared glasses can be expressed as $Na_2O{\cdot}CaO{\cdot}2SiO_2{\cdot}xZnO$, where $x = 0.00$, 0.17, 0.34, and 0.68. The SEM micrograph and EDS analysis of all as-quenched glasses reveal a homogeneous distribution of the elements.

Thermal Analysis. The DTA curves of the glasses analyzed are shown in Figure 1, and the glass-transition (T_g), crystallization (T_c), and melting temperatures are summarized in Table 4. The inflection point at the endothermic shoulder of the DTA curves in the range 494−510 °C enables the evaluation of the T_g; however, the values reported in Table 4 were determined from the DSC curves. Figure 1 shows that the exothermic peak at 661°, characteristic of the S50 glass, shifts to slightly higher values in zinc-containing glasses; for $x = 0.34$, the base of the peak becomes very large ($\Delta T = 200$ °C). Moreover, two other peaks appear at lower temperature (578 and 613 °C) for $x = 0.68$ (Table 4). The exothermic peaks are assigned to glass crystallization, and to identify the crystalline phases, we carried out an isothermal treatment at a temperature corresponding to the maximum of the DTA analysis or to the first maximum in the case of $x = 0.68$; the temperature was kept constant for 2

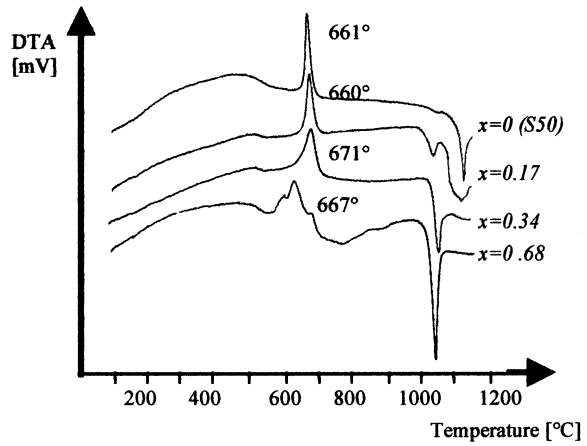

Figure 1. DTA curves of the $Na_2O{\cdot}CaO{\cdot}2SiO_2{\cdot}xZnO$ glasses.

TABLE 4: Glass-Transition (T_g), Crystallization (T_c), and Melting (T_m) Temperatures for the Investigated Glasses

	T_g (°C) ± 2	T_c (°C) ± 2	T_m (°C) ± 2
$x = 0$ (S50)	510	661	1080, 1162
$x = 0.17$	496	672	1067, 1180
$x = 0.34$	495	669	1084
$x = 0.68$	494	578, 613, 667	1077

TABLE 5: Experimental and Calculated[21] Density for the Investigated Glasses

	mol % ZnO ± 0.1	exptl density (g/cm^3) ± 0.002	Appen density (g/cm^3)	Huggins density (g/cm^3)
$x = 0$ (S50)	0	2.718	2.72	2.77
$x = 0.17$	4.2	2.810	2.84	2.80
$x = 0.34$	8.0	2.894	2.91	2.82
$x = 0.68$	14.5	3.028	3.04	3.01

h 30 min. After the thermal treatment, the samples turned opaque. At temperature values above 1060 °C, the DTA analysis shows one or two endothermic peaks assigned to the melting process. The addition of zinc oxide to S50 produces a lowering of T_g, from 510 to 496 °C measured for $x = 0.17$; on further increasing of zinc content, the T_g remains constant. This result suggests that the overall effect of ZnO addition is weakening of the glass network; however, the perturbation induced is not proportional to zinc concentration. In fact, the first addition of small amounts of zinc to the soda-lime glass produces a remarkable perturbation of the network, while a compensative effect seems to become operative at higher concentration of zinc.

The behavior of the crystallization temperature (T_c) is opposite to the behavior of the T_g; in fact zinc-containing glasses require a higher temperature to crystallize: T_c ranges from 661 °C for S50 to 669−672 ± 2 °C for $x = 0.34$ and 0.17, respectively. Therefore, we can assume that the crystal phases formed in the zinc-free glass are also present in glasses with low zinc content. Moreover, besides the peak at 667 °C, two additional lower temperature peaks are observed for $x = 0.68$. This might suggest that other phases are formed at lower temperature, as also supported by the broaden peak observed for $x = 0.34$ (Figure 1).

Density. The experimental density (Table 5) of the glasses increases linearly with zinc concentration. The correlation coefficient (r) obtained, $r = 0.999$, is worth noting and suggests that the concentration of zinc oxide does not influence its role in the glass, as well as its coordination geometry, which is maintained over the whole range of compositions. Therefore, the linear dependence of density with ZnO concentration seems to be the result of the difference in the atomic mass of zinc with respect to the atomic masses of sodium, calcium, and silicon. The density calculated by the Appen method,[21] based on the additivity of the contributions due to each oxide, gives rise to a straight line with $r = 0.991$ fairly parallel to the experimental one. A similar behavior with a worse correlation coefficient ($r = 0.871$) is obtained when density is calculated by means of the Huggins method,[21] the difference in the values calculated for the same compositions by means of the two methods being within 3%.

XRD Powder Diffraction. The XRD pattern of as-quenched glasses is typical of amorphous materials and shows a broad signal centered at 2.81−2.83 Å, as previously found in alkali-silicate glasses,[22] and a second very weak signal at about 4.17 Å, characteristic of glassy silica.

The XRD pattern of the powders obtained after the thermal treatment of the S50 glass reveals the presence of a crystalline species, $Na_2Ca(SiO_3)_2$,[23] identified on the basis of the intensity and position of the signals. In all zinc-containing glasses, in addition to the previous phase, we identified zinc-containing phases: $Na_4Zn_2Si_3O_{10}$[24] and Na_2ZnSiO_4.[25] With increasing zinc content, the signals due to $Na_2Ca(SiO_3)_2$ decrease and the signals characteristic of Na_2ZnSiO_4 increase; therefore, for $x = 0.68$, the $Na_2Ca(SiO_3)_2$ and Na_2ZnSiO_4 phases can be considered comparable. The ZnO glass content seems not to influence strongly the signals due to $Na_4Zn_2Si_3O_{10}$. Moreover, CaO[26] and $Ca_6(SiO_4)(Si_3O_{10})$[27] are found for the $x = 0.68$ composition as minor phases. The XRD analysis on the quenched glass containing 15.5 mol % ZnO revealed the presence of the Na_2ZnSiO_4 as the main phase and of the $Na_2Ca(SiO_3)_2$ and $Ca_6(SiO_4)(Si_3O_{10})$ phases.

The crystal structures of both $Na_2Ca(SiO_3)_2$[28] and Na_2ZnSiO_4[29] are known. The $Na_2Ca(SiO_3)_2$ crystal structure is built up of stacked six-member puckered silicate rings of formula $[Si_6O_{18}]^{12-}$, sodium, and calcium ions. The rings have a symmetrical form and are stacked in a cubic-close-packed fashion along the c axis direction and are held together by Na and Ca ions, which are located at four distinct positions (M(1), M(2), M(3), M(4)). The crystal packing is due to the bonding interactions and van der Waals contacts involving sodium and calcium ions and oxygens; the alkaline and alkaline-earth cations are bonded to oxygen atoms of the fundamental set, to symmetry-related oxygens belonging to stacked rings, and finally to oxygens from approximately adjacent rings (the Na−O and Ca−O distances of ≤2.70 Å were considered, coherently with the ionic radii values[30]). The O(1) bridging oxygens (BO, oxygens bound to two network-former ions) bind the cations of the fundamental set at the M(3) site and form a second bond of the same length with the symmetry-related M(3) cation; in addition, O(1) forms four identical bonds with the symmetry-related Na^+ at the M(2) site. The NBO O(2) and O(3) atoms form nine bonds with the four independent cations; O(3) forms also short van der Waals contacts (M···O(3) range 2.720−3.144 Å). Both sodium and calcium ions display distorted geometries with the following coordination numbers: four (Na^+ and Ca^{2+} at M(3) site), six (Na^+ and Ca^{2+} at M(1) site and Ca^{2+} at M(4) site), and eight (Na^+ at M(2) site) and mean distances within each coordination polyhedron in the range 2.32−2.68 Å. Additional information with respect to the published structure can be derived[31] by calculating the mean, the coordination number of metal ions, and the metal−oxygen distances. By approximating to 0.25 the population of Na ions at the M(1) and M(3) sites, to 0.10 and 0.25, respectively, those of Ca ions at the same sites, and to 0.5 the population of Na^+ at M(2),[31]

TABLE 6: Structural Parameters Derived from MD Simulations of the Glasses and Structural Parameters for the Crystal Phases[28,29] Obtained by Glass Crystallization

	MD												
	bond lengths (Å)				bond angles (deg)						interatomic distances (Å)		
	Si−O	Zn−O	Ca−O	Na−O	O−Si−O	O−Zn−O	Si−O−Si	Si−O−Zn	O−Ca−O	O−Na−O	O−O	Zn−Zn	Si−Zn
$x = 0$ (S50)	1.58		2.23	2.46	108		150		94	56−98	2.58		
$x = 0.17$	1.58	1.95	2.26	2.46	108	109	153	134	88	56−95	2.56	3.12	3.25
$x = 0.34$	1.58	1.94	2.25	2.46	108	106	150	133	88	56−95	2.57	2.83, 3.20	3.18
$x = 0.68$	1.57	1.93	2.24	2.45	108	107	146	126	88	57−95	2.56	3.14	3.25

	Crystal Structure													
	bond lengths (Å)				bond angles (deg)						coordination number			
phase	Si−O	Zn−O	Ca−O	Na−O	Si−O−Si	O−Si−O	Si−O−Zn	Na(1)−O−Na(2)	O−Na−O	O−Zn−O	Si	Zn	Ca	Na
$Na_2Ca(SiO_3)_2$	1.601		2.41[a]	2.56[a]	156	109					4		5.0[a]	6.5[a]
Na_2ZnSiO_4	1.64	1.95		2.32		110	128	89	109	109	4	4		4

[a] Data values calculated in the present work from the crystal coordinates given in ref 28.

we obtain the value of 6.5 and 5.0 for the mean coordination number of Ca^{2+} and Na^+ ions, respectively. The mean M−O distances are 2.56 and 2.41 Å for Na^+ and Ca^{2+}, respectively. Table 6 lists the mean structural parameters of $Na_2Ca(SiO_3)_2$ and of Na_2ZnSiO_4. The mean Si−O bond length for the three independent SiO_4 tetrahedra is 1.60 Å,[28] the O−Si−O bond angles are centered at 109°,[28] and the Si−O−Si angles between connected tetrahedra are centered at 159°.[28]

The structure of Na_2ZnSiO_4[29] is described as formed by alternate ZnO_4 and SiO_4 corner-sharing tetrahedra. Two independent sodium cations display an essentially tetrahedral geometry with mean Na(1)−O = 2.35 Å and Na(2)−O = 2.29 Å[29] distances and a mean O−Na−O angle of 109°[29] calculated for Na(1) and Na(2), respectively. The mean O−Si−O angle is 110°, and the mean O−Zn−O angle is 109°.[29] Each oxygen atom forms four bonds to the four independent Zn, Si, Na(1), and Na(2) atoms and a contact with a sodium atom. The structure is built up of a pyroxene-like cationic chains of Na tetrahedra and an anionic one of Zn tetrahedra interconnected with Si tetrahedra to form a tridimensional network. The mean Si−O and Zn−O bond distances are 1.64 and 1.95 Å,[29] respectively.

The $Na_4Zn_2Si_3O_{10}$ was found[32] to be formed by quenching at 1125 K a melt of which the stoichiometry is written as $Na_xZn_{x/2}Si_{2-x/2}O_4$, for $1.65 < x < 1.75$; for $2.0 < x < 1.70$, the crystallization of the melt gives rise to Na_2ZnSiO_4. This last phase is also formed for $1.65 < x < 1.75$ if the quencing temperature is lower than 1125 K. $Na_4Zn_2Si_3O_{10}$ differs from Na_2ZnSiO_4 essentially in view of the Si/Zn ratio value, which is equal to 1.5 in the former and to 1 in the latter, but the ratio O/Zn + Si is the same; therefore, a tetrahedral coordination geometry for the zinc ion can be proposed also for this phase.

It is generally assumed[33] that the local structure of a glass is similar to that of the phases separated by glass crystallization, although in multicomponent glasses the different phases should be mixed to reach a monophasic system. Therefore, a rationalization of the glass chemical properties can be attempted on the basis of the knowledge of the compositionally equivalent crystalline phases. The linear correlation observed between density and ZnO concentration is in line with the higher density of Na_2ZnSiO_4 (3.4 g/cm^3)[29] as compared to $Na_2Ca(SiO_3)_2$ (2.817 g/cm^3),[28] due both to the high atomic zinc mass and to the extremely compact structure of Na_2ZnSiO_4, the network of which requires all of the oxygens to be shared between adjacent tetrahedra. The partial destruction of the $Na_4Ca_4(SiO_3)_6$-like arrangement in the glass as a consequence of the insertion of the Na_2ZnSiO_4-like and $Na_4Zn_2Si_3O_{10}$-like phases might be responsible for the T_g decreasing on going from the zinc-free glass S50 to zinc-containing glasses. At increasing ZnO content, the T_g decrease becomes negligible probably because the consumption of the $Na_2Ca(SiO_3)_2$-like phase and the destruction of its arrangement is counterbalanced by the formation of a significant amount of the strongly interconnected zinc-containing phases. Finally, an explanation for the behavior of the crystallization temperature of the glass with $x = 0.68$ can be provided. In fact, literature data[32] report that Na_2ZnSiO_4 can be obtained using a quenching temperature as low as 552 °C, so the crystallization peak at 578 °C can be assigned to Na_2ZnSiO_4; the increased amount of this compound with increasing zinc content is suggested from the broadening of peak profile for $x = 0.34$.

Molecular Dynamics Simulations. The information derived from the analysis of the crystalline phases of these glasses can be combined with atomistic computer simulations to provide deeper insight into the amorphous structure. In fact, the qualitative concepts at the basis of the modified random network model of glass structure put forward by Greaves[34] can be easily investigated with molecular dynamics thecniques. According to Greaves's model, the alkali ions are not uniformily distributed throughout the tetrahedral network but rather are clustered inhomogeneously forming alkali-rich regions and silica-rich regions. This is consistent with the information derived from the analysis of the crystalline phases obtained from the glasses studied, because no mixed phases containing Zn, Ca, and Si are observed.

A picture of the local structure of the glasses can be obtained from the molecular dynamics trajectories by analyzing the coordination number and bond length and bond angle distribution functions, while the analysis of the Q^n species distribution can be helpful for deciphering the network organization of the medium-range order glass structure. This index is defined as the number of bridging oxygens surrounding a network former ion. In the present work, the definition of the oxygen types is based on the network-former (Si or Zn) ion−oxygen bond distance: the nonbridging oxygens (NBO) are species linked to one network-former ion, the bridging oxygens (BO) are oxygens linked to two network-former ions, and finally three-bridging oxygens (TBO) are oxygens linked to three network-former ions, provided that each of the former species is properly coordinated.[18]

Coordination Number Distribution. Table 7 lists the coordination number (CN) distribution for the different ions in the series of glasses studied. The CN has been obtained by integration to the first minimum (r_{cutoff}) in the pair distribution

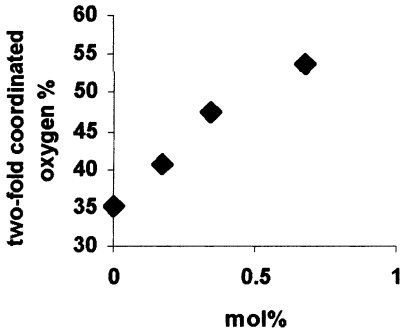

Figure 2. Percentage of 2-fold coordinated oxygens versus composition.

TABLE 7: Percentage Contribution to the Si, Zn, O, Ca, and Na Coordinations as a Function of Zinc Addition to the Soda-Lime S50 Glass

CN	Si	Zn	O	Ca	Na
		$x = 0$ (S50)			
1			64.79		
2			35.21		0.02
3					0.94
4	96.7			16.62	11.25
5	3.3			48.27	36.69
6				30.51	34.99
7				4.12	13.04
8				0.48	2.55
9				0.01	0.51
mean	4.03		1.34	5.24	5.58
		$x = 0.17$			
1			58.98		
2			40.8		
3		1.19	0.22		0.88
4	95.67	92.32		10.03	12.05
5	4.33	6.49		48.78	3.93
6				30.31	32.51
7				9.95	16.76
8				0.92	3.60
9					0.26
mean	4.04	4.05	1.41	5.43	5.54
		$x = 0.34$			
1			51.48		
2			47.57		
3		1.32	0.95	0.01	0.53
4	96.37	84.85		12.96	10.18
5	3.66	13.83		41.19	33.55
6				36.44	34.33
7				8.97	18.71
8				0.36	2.64
9				0.07	0.06
mean	4.04	4.13	1.49	5.43	5.69
		$x = 0.68$			
1			41.76		
2			53.78		
3		2.18	4.46		0.12
4	94.70	87.21		4.97	6.60
5	5.30	10.57		32.30	29.43
6		0.02		44.33	35.50
7				15.48	21.79
8				2.84	5.27
9				0.08	1.18
mean	4.05	4.08	1.62	5.79	5.93

function curves. Thus, the r_{cutoff} for Si−O is 2.2 Å, for Na−O is 3.0 Å, for Ca−O is 3.0 Å, and for Zn−O is 2.5 Å. A compositional dependence is observed for the CN distribution of the O, Ca, and Na species. In particular, a linear trend can be detected in the percentage of 2-fold coordinated oxygens, which increases with zinc addition (Figure 2). Moreover, a small percentage of 3-fold coordinated oxygens is observed for the $x = 0.68$ composition. The CN distribution for the Na and Ca species shows a shift in the percentage of occupancy from the 5-fold toward the 6-fold (Ca) and 7-fold (Na) sites as a function of Zn addition.

The Si and Zn species manifest a clear preference to occupy 4-fold sites over all of the compositional range considered, in full agreement with the coordination assumed in the crystal phases isolated (Table 6). However, zinc addition to soda-lime silicate glass S50 induces significant changes in the local oxygen ions environment, as it is detected by the analysis of the NBO, BO, and TBO species contributions to the Si and Zn coordination (Table 8).

As expected, the high content of Na and Ca ions in the silicate glass S50 is responsible for the significant percentage of Si−NBO sites, which confers disorder in the network. Zn addition reduces the Si−NBO content and increases the percentage of Si−BO and Si−TBO species. The main contribution to the zinc ion coordination is ascribed to the BO species, implying its network-former structural role in these glasses. It is interesting to note that the percentage of Zn−BO species decreases progressively with zinc addition, while a complementary increase in the Zn−TBO is observed. Moreover, the percentage of NBO species associated with Ca is always significantly higher than the percentage of NBO associated with Na, and the NBO/BO ratio of neighboring O of Na levels down to 1 when the highest concentration of zinc ions is reached in the glass.

These results are consistent with previous molecular dynamics simulations carried out on sodium zinc silicate glasses,[11] where the clustering effect of sodium around tetrahedrally coordinated zinc was claimed to account for the positive charge deficiency associated with a ZnO_4 tetrahedron. A similar charge compensation phenomenon was observed in soda-lime[35] and sodium alumino-silicate glasses.[36]

Bond Length and Bond Angle Distribution. No significant compositional dependence on the bond lengths is observed in the series of glasses studied; however, Zn addition to the S50 glass induces a modification of the shape of the Ca−O and O−O peaks, as shown in Figure 3, in which the Si−O, Zn−O, Na−O, Ca−O, and O−O pair distribution functions are reported for the $x = 0.00$ and $x = 0.68$ glass compositions. The shape of the Si−O and Zn−O first peak indicates an ordered local environment, characteristic of network-forming atoms, while the Na−O pair shows a broader peak of lower amplitude, characteristic of a network modifier. The Ca environment seems to be more ordered than the Na one, the Ca−O peak being significantly sharper. The average Si−O distance (1.58 Å) is slightly shorter than the distances observed in the crystal phases (1.62−1.64 Å, see Table 6) isolated from the glasses. The high percentage of alkali/alkaline-earth oxides present in the glasses might be considered responsible for the reduced bond length, because Si−NBO is generally found to be shorter than Si−BO.[37] The average Zn−O distance (1.94 Å) compares well with the distance found in the Na_2ZnSiO_4 (see Table 6) and is characteristic of ZnO_4 tetrahedra linked to silicate tetrahedra.[38] This is consistent with the asymmetry of the Zn−O first peak manifested in Figure 3, which indicates that the shape of the Zn tetrahedra in the simulated glass is somewhat distorted. In fact, the O−Zn−O bond angle shows a broad distribution (full with at half-maximum, fwhm, 30°) with a maximum at around 109° and an asymmetry toward lower angles, probably due to the formation of Zn−TBO species (Figure 4). Moreover, average values of the Zn−Zn, Si−Zn, and O−O neighbor peaks (Table 6) are indicative of a typical disordered arrangement of ZnO_4

TABLE 8: Percentage Contributions (%) of NBO, BO, and TBO to the Si, Zn, Ca, and Na Coordination

	Si−O			Zn−O			Ca−O			Na−O		
	NBO	BO	TBO	NBO	BO	TBO	NBO	BO	TBO	NBO	BO	TBO
$x = 0$ (S50)	51.3	48.7	0				93.8	6.2	0	79.6	20.4	0
$x = 0.17$	48.6	51.2	0.2	6.2	90.8	3.0	88.6	11.4	0	69.5	30.4	0.1
$x = 0.34$	42.6	56.4	1.0	6.7	88.1	5.2	81.4	18.5	0	62.8	36.7	0.5
$x = 0.68$	36.0	60.3	3.7	5.4	76.0	18.6	72.0	26.3	1.7	50.5	47.6	1.9

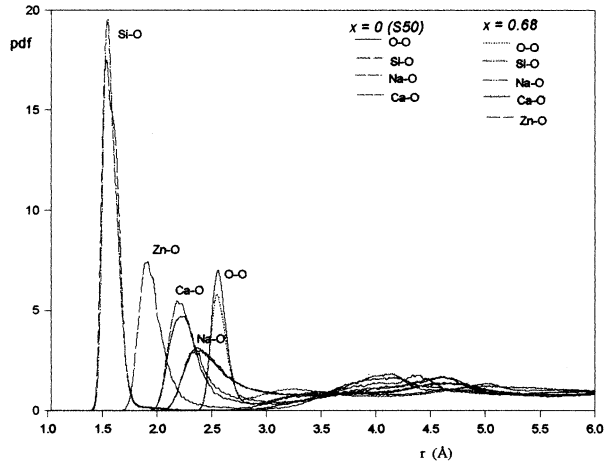

Figure 3. Si−O, Zn−O, Ca−O, Na−O, and O−O pair distribution functions for the $x = 0$ (S50) and $x = 0.68$ glass compositions.

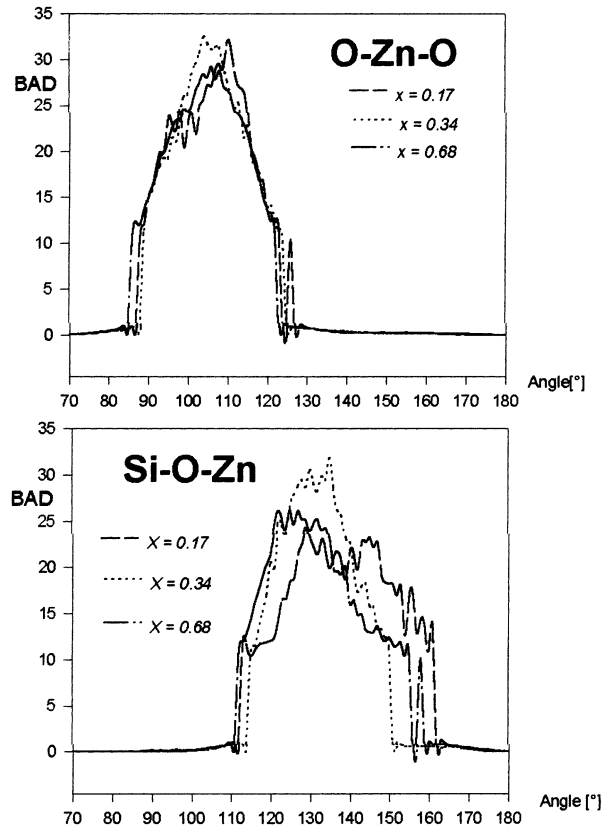

Figure 4. Bond angle distributions for the Si−O−Zn and O−Zn−O angles.

and SiO_4 corner-sharing tetrahedra,[11] as supported also by the broad distribution of Si−O−Si and Si−O−Zn angles. In fact, the average Si−O−Si angle (150°) is typical of disordered arrangements of corner-sharing tetrahedra.[39] Moreover, a compositional dependence is observed for the Si−O−Zn angle

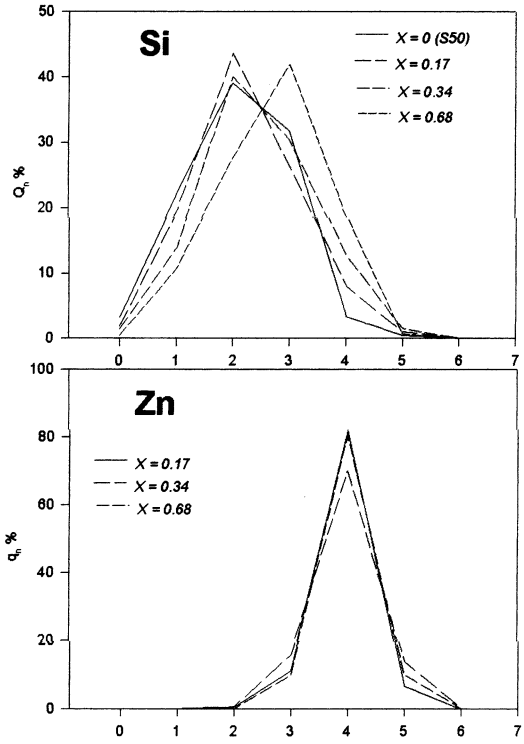

Figure 5. Q^n species distribution of Si (Q^n) and of Zn (q^n).

distribution, which shows a shift toward lower angles and a progressive narrowing of the peak as a function of zinc addition to the soda-lime parent glass (Figure 4). The value of 126° observed for the Si−O−Zn maximum of the $x = 0.68$ composition compares well with the value observed in the Na_2ZnSiO_4 crystal.

The local environment of sodium and calcium provides information on the degree of local disorder, which is of great interest when comparing the structural arrangements of different glasses. The average Ca−O bond distance found in the simulations (2.25 Å) is slightly shorter than the one found in the $Na_2Ca(SiO_3)_2$ crystal phase (2.39 Å), and the O−Ca−O bond angle distribution shows a broad peak (fwhm 40°) with the maximum at around 88° in zinc-containing glasses. Visual inspection of the glasses obtained by the simulations shows that, although the average CN is consistent with the CaO_6 coordination largely found in crystals,[40] the environment around Ca, mainly constituted by NBO species, is considerably disordered.

A mixing behavior results from the simulations for the sodium ions. In fact, according to a recent combined multiple-quantum magic-angle spinning (MQ-MAS) NMR and molecular dynamics study, Na modifiers are characterized by (a) a radial distribution function with the oxygen shifted to lower distances and (b) a lower coordination with formers with respect to Na charge compensator.[41]

A shift toward larger coordination is indeed observed in the present study as a function of Zn addition to soda-lime S50 glass (Table 7), which emphasizes the Na charge compensator

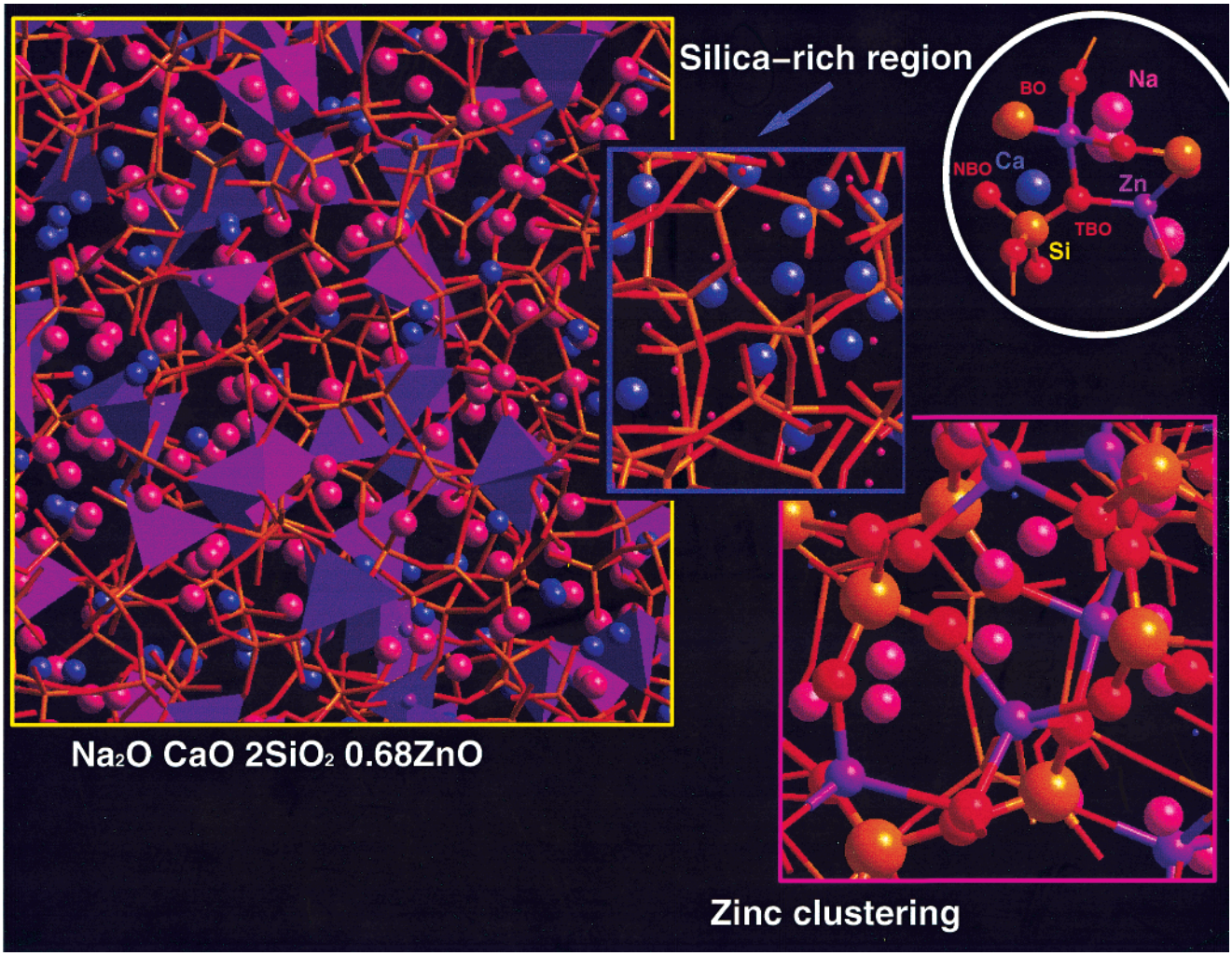

Figure 6. Representation of a slice of the simulated $Na_2O{\cdot}CaO{\cdot}2SiO_2{\cdot}0.68ZnO$ glass.

role. On the contrary, the Na−O radial distribution function tends to classify it as modifier.

The average Na−O bond distance (2.46 Å) found in the simulations lies within the one found in the Na_2ZnSiO_4 (2.35 Å) and $Na_2Ca(SiO_3)_2$ (2.56 Å) crystalline phases. In general in glasses, an increase in the Na−O distance should be expected when a second network former is added to the glass composition.[41] In fact, a difference of about 0.4 Å in the Na−O distance, depending on whether the O is bridging or nonbridging, has been revealed by NMR spectroscopy.[41] The order of magnitude of this difference corresponds to the results observed here for the soda-lime glass. The deconvolution of the Na−O peak gives distances of 2.37 Å for Na−NBO and of 2.72 Å for Na−BO. However, zinc addition does not influence significantly the Na−NBO bond lengths, while it produces a small decrease of the Na−BO and the formation of low percentages of Na−TBO with increased bond lengths. This might be indicative of a preference for the Na ions to be closer to the Zn network former with respect to the Si species, because in the Zn tetrahedra the central cation is farther from the neighboring oxygen atoms, allowing the Na charge compensator to find closer positions.

Q^n Distribution. The Q^n species distribution furnishes a measure of the connectivity of the glass network. This index is defined as the number of bridging oxygens surrounding a network former ion; therefore, the $n = 0$ corresponds to the isolated tethrahedron, $n = 1$ to the tetrahedron-terminating chain, $n = 2$ to the in chain tetrahedron, $n = 3$ to the tetrahedron forming a branching point, and finally $n = 4$ to the tetrahedron in which all four oxygens are bridging ones. The analysis has been performed on the Si (Q^n) and the Zn ions (q^n), and the results are reported in Figure 5 for the compositions studied.

The principal q^n species for Zn is four for all of the compositions, while the relative population of the Q^n species for Si is composition-dependent. Because of the high percentage of alkali/alkaline-earth content, a broad distribution over the Q^1, Q^2, and Q^3 species for the Si in the S50 basic system is observed, with a maximum for the Q^2, while only a small amount of Q^4 species are detected. Small percentages of Zn addition produce a decrease in the percentages of Q^1 and Q^3 species to favor the Q^4 and, to a smaller extent, Q^2 sites. A significant shift in the equilibrium toward the Q^3 and Q^4 species is obtained for high percentages of Zn addition ($x = 0.50$).

This behavior can be better understood by a visual analysis of the simulated structures; in fact, in the $x = 0.12$ and $x = 0.25$ glasses, the Zn atoms are randomly dispersed in the silicate three-dimensional network, and Zn tetrahedra units are interconnected with SiO_4 tetrahedra. The $x = 0.50$ glass shows a different picture. Pairs of corner-sharing ZnO_4 tetrahedra start to form in the glass and give rise to long strips of $[(ZnO_4)_n-(SiO_4)_N]_m$ tetrahedra. Moreover, distinct regions can be observed in the glass, a zinc-rich region and a silicon-rich region where Ca ions are preferentially found (Figure 6).

Conclusions

It is generally assumed that a reasonable rationalization of the structure of glass can be derived from the analysis of compositionally equivalent crystalline phases, because several silicate glasses containing alkaline/alkaline-earth cations and transition metals have a degree of local and medium-range ordering that is strongly reminiscent of compositionally equivalent crystalline phases.[33] The approach presented here combines the information derived from the analysis of the crystal phases obtained from the quaternary glasses and those derived from molecular dynamics simulations to obtain an understanding of the glass structure at the atomic scale.

The scenario that emerges is unequivocal in assigning to the zinc ions a specific structural role and a preference for the tetrahedral coordination for the full range of compositions studied. The Zn tetrahedra have longer average cation−oxygen distances with respect to Si, and the internal bonding is weaker with respect to the surrounding silicate tetrahedra. A clustering effect of Na around Zn tetrahedra is observed and provides compensation for the positive charge deficiency. On the other hand, the Ca ions manifest a strong propensity for coordination by NBO of the silicate network, which may be explained in terms of its field strength.[21] Therefore, the modified random network model[34] well depicts the medium-range structure of these glasses. The progressive addition of zinc oxide causes an overall decrease of NBO species and a total rearrangement of the glass structure in which segregation zones of calcium modifiers and Si−NBO can be found. Moreover, the $x = 0.50$ glass, which contains the experimentally determined maximum zinc content compatible with glass structure, shows clusters of Si−O−Zn islets of considerable size with consequent migration of Na ions to the interior of the zinc−silicate cages. A significantly larger structural disorder of the sodium around the tetrahedral Zn sites is observed in the glass with respect to the crystal phase. In fact, the oxygens pack less closely around Na, leading to somewhat larger coordination numbers.

In conclusion, the results of the molecular simulations study provide a rationale for the limit of solubility of ZnO in the soda-lime glass considered and for the crystallization behavior of the zinc-containing glasses. Moreover, the T_g behavior might be explained by invoking an initial weakening of the soda-lime silicate network due to the insertion of Zn−O bonds, which are weaker than Si−O, followed by the progressive complexation of the network, as highlighted by the increased percentages of the TBO species and the shift of Q^n toward higher values as a function of Zn addition to the soda-lime glass. Finally, the compact network structure obtained explains the linear relationships observed between the measured densities and the glass composition. This is due to the geometries of the Zn tetrahedra that present longer cation−oxygen distances and smaller angles with respect to Si tetrahedra and to the angle between interconnected Si−Zn tetrahedra, which decreases significantly with zinc addition, reducing the volume between linked tetrahedra units.

Acknowledgment. The authors thank C.I.G.S. for supplying the SEM−EDS instrument, C.I.C.A.I.A. for the Cerius2 program and computational facilities, and Prof. M. Saladini for structural calculations.

References and Notes

(1) Ennas, G.; Musinu, A.; Piccaluga, G.; Montenero, A.; Gnappi, G. *J. Non-Cryst. Solids* **1990**, *125*, 181.
(2) Onyiriuka, E. C. *J. Non-Cryst. Solids* **1993**, *168*, 268.
(3) Rosenthal, A. B.; Garofalini, S. H. *J. Non-Cryst. Solids* **1986**, *87*, 254.
(4) Aylett, B. J. *The Chemistry of Zinc, Cadmium and Mercury*; Pergamon Press: Exeter, U.K., 1975; Chapter 2.
(5) Syono, Y.; Akimoto, S.; Matsui, Y. *J. Solid State Chem.* **1971**, *3*, 369.
(6) Battaglia, L. P.; Bonamartini Corradi, A.; Menabue, L.; Saladini, M. *Inorg. Chim. Acta* **1985**, *107*, 73.
(7) Vogel, W. In *Chemistry of Glass*; Lense, E., Ed.; American Ceramic Society: Columbus, OH, 1985.
(8) Pesina, T. I.; Zakreuska, V. A.; Puken O. P. *J. Am. Ceram. Soc.* **1984**, *67*, 47.
(9) Dumas, T.; Petiau, L. J. *J. Non-Cryst. Solids* **1986**, *81*, 201.
(10) Matsubara, E.; Waseda, Y.; Ashizuka, M.; Ishida, E. *J. Non-Cryst. Solids* **1988**, *103*, 124.
(11) Rosenthal, A. B.; Garofalini, S. H. *J. Am. Ceram. Soc.* **1987**, *70*, 821.
(12) Newell, R. G.; Feuston, B. P.; Garofalini, S. H. *J. Mater. Res.* **1989**, *4*, 434.
(13) Kim, H. M.; Miyaji, F.; Kokubo, T.; Ohtsuki, C.; Nakamura, T. *J. Am. Ceram. Soc.* **1995**, *78*, 2405.
(14) Nardelli, M. *Comput. Chem.* **1993**, *7*, 95.
(15) Smith, W.; Forester, T. R. *J. Mol. Graphics* **1996**, *14*, 136.
(16) *Cerius2*; Molecular Simulations Inc.: San Diego, CA, 1997.
(17) Vessal, B. *J. Non-Cryst. Solids* **1994**, *177*, 103.
(18) Cormack, A. N.; Cao, Y. *Mol. Eng.* **1996**, *6*, 183.
(19) Lewis, G. V.; Catlow, C. R. A. *J. Phys. C: Solid State Phys.* **1985**, *18*, 1149.
(20) Montorsi, M.; Menziani, M. C.; Leonelli, C.; Du, J.; Cormack, A. N. *Phys. Chem. Glasses* **2002**, *43*, 145.
(21) Volf, M. B. *Mathematical Approach to Glass*; Glass Science and Technology, Vol. 9; Elsevier: Prague, Czech Republic, 1988; and references therein.
(22) Volf, M. B. *Chemical Approch to Glass*; Glass Science and Technology, Vol. 7; Elsevier: Amsterdam, 1984.
(23) World Wide Web Mincryst-Crystallographic Database for Minerals, 4882 CPDS No. card. http://database.iem.ac.ru/mincryst (January 15, 2002).
(24) *Powder Diffraction File, Inorganic Phases* Powder Diffraction File No. 37-409, JCPDS-ICDD, Joint Committee of Powder Diffraction Standards: Swarthmore, PA, 1989.
(25) *Powder Diffraction File, Inorganic Phases* Powder Diffraction File No. 37-407, JCPDS-ICDD, Joint Committee of Powder Diffraction Standards: Swarthmore, PA, 1989.
(26) *Powder Diffraction File, Inorganic Phases* Powder Diffraction File No. 29-370, JCPDS-ICDD, Joint Committee of Powder Diffraction Standards: Swarthmore, PA, 1989.
(27) *Powder Diffraction File, Inorganic Phases* Powder Diffraction File No. 37-1497, JCPDS-ICDD, Joint Committee of Powder Diffraction Standards: Swarthmore, PA, 1989.
(28) Ohsato, H.; Takeuchi, Y.; Maki, I. *Acta Crystallogr., Sect. C* **1986**, *C42*, 934.
(29) Plakhov, G. F.; Belov, N. V. *Sov. Phys. Crystallogr.* **1979**, *24* (6), 674.
(30) Shannon, R. D. *Acta Crystallogr.* **1976**, *A32*, 751.
(31) The atom and site numbering is taken from ref 29. The geometric data are calculated in the present work from the coordinates given in ref 29.
(32) Grins, J. *Solid State Ionics* **1982**, *7*, 157.
(33) Gaskell, P. H. *J. Non-Cryst. Solids* **1995**, *192*−*193*, 9.
(34) Greaves, G. N. *J. Non-Cryst. Solids* **1985**, *71*, 203.
(35) Cormack, A. N.; Du, J. *J. Non-Cryst. Solids* **2001**, *293*−*295*, 283.
(36) Leonelli, C.; Lusvardi, G.; Montorsi, M.; Menziani, M. C.; Menabue, L.; Mustarelli, P.; Linati, L. *J. Phys. Chem. B* **2001**, *105*, 919.
(37) Yuan, X.; Cormack, A. N. *J. Non-Cryst. Solids* **2001**, *283*, 69.
(38) McKeown, D.; Muller, I. S.; Buechele, A. C.; Pegg, I. L. *J. Non-Cryst. Solids* **2000**, *261*, 155.
(39) Mozzi, R. L.; Warren, B. E. *J. Appl. Crystallogr.* **1969**, *2*, 164.
(40) Gaskell, P. H.; Eckersley, M. C.; Barnes, A. C.; Chieux, P. *Nature* **1991**, *350*, 675.
(41) Angeli, F.; Delaye, J.-M.; Charpentier, T.; Petit, J.-C.; Ghaleb, D.; Faucon, P. *J. Non-Cryst. Solids* **2000**, *276*, 132.